ISSN: 3033-3652

Journal of Physical Mathematics & its Applications

Research Article

Open Access

A Regularized Urysohn Operator Framework for Nonstationary AP/HTPB Solid-Propellant Combustion with Memory Effects, Spectral Analysis and Artificial Intelligence

Manuel J Alves* and Elena V Molchanova Alves

Instituto Superior de Ciências e Tecnologia de Moçambique

ABSTRACT

This paper develops a regularized nonlinear Urysohn-operator framework for nonstationary ammonium-perchlorate/hydroxyl-terminated-polybutadiene (AP/HTPB) solid-propellant combustion with hereditary thermal feedback, pressure coupling and delayed response. The state is governed by a causal nonlinear integral equation whose kernel depends on time, history, temperature-sensitive kinetics and the current magnitude of the state. The regularized model is written as $u_\varepsilon + \varepsilon L u_\varepsilon = f + U(u_\varepsilon)$, where L is a positive spectral operator and $\varepsilon > 0$ is a smoothing parameter. Beyond standard existence and uniqueness results, the article establishes exponential stability, robustness with respect to perturbations of the kernel, the explicit estimate $\|u_\varepsilon - u\| \le C\varepsilon$, differentiability of the solution with respect to model parameters, eigenvalue localization, a spectral-radius bound and pseudospectral resolvent estimates. A numerical study compares short and long memory, strongly nonlinear saturated kernels, several regularization levels and five iterative solvers. Three-dimensional response surfaces, a spectral plot, a heat map and sensitivity diagrams illustrate the theory. The framework is also connected with DeepONet, Fourier neural operators, physics-informed neural operators and transformer memory. The resulting model provides an analytically transparent and computationally stable bridge between nonlinear integral equations, combustion dynamics and modern operator learning.

***Corresponding author**
Manuel J Alves, Instituto Superior de Ciências e Tecnologia de Moçambique.

Received: March 01, 2026; **Accepted:** September 10, 2026; **Published:** September 23, 2026

Keywords: Urysohn Operator, Nonlinear Integral Equation, AP/HTPB Combustion, Memory Effects, Regularization, Exponential Stability, Pseudospectrum, Neural Operator, DeepONet, Fourier Neural Operator

MSC 2020: 45G10; 47H10; 47H30; 65R20; 80A25; 68T07.

Introduction

Solid-propellant combustion is governed by strongly coupled heat transfer, condensed-phase decomposition, gas generation, surface regression, chamber pressure and acoustic feedback. In AP/HTPB composites, the response observed at the burning surface is not purely instantaneous. Heat penetrates the condensed phase, chemical intermediates accumulate, and the effective burning rate retains information from previous states. A nonlinear memory operator is therefore a natural modelling device.

Let $I = [0, T]$ and $X = C(I)$ with the supremum norm. The baseline equation is

$$u(t) = f(t) + \int_0^t K(t, s, u(s); \theta)\, \mathrm{d}s, \tag{1.1}$$

where f represents external forcing, K is a causal nonlinear kernel and θ collects physical parameters.

The regularized equation is

$$u_\varepsilon + \varepsilon L u_\varepsilon = f + U_\theta(u_\varepsilon), \qquad \varepsilon > 0, \tag{1.2}$$

with L positive. The spectral factor $(I + \varepsilon L)^{-1}$ damps unresolved high-frequency modes and improves conditioning.

The main contributions are: (i) a complete fixed-point formulation with explicit hypotheses; (ii) an exponential-stability theorem; (iii) a kernel-perturbation robustness estimate; (iv) an $O(\varepsilon)$ convergence theorem; (v) differentiability with respect to physical parameters; (vi) localization of the spectrum and a spectral-radius criterion; (vii) a resolvent and pseudospectral analysis; (viii) numerical comparisons of memory regimes and solvers; and (ix) a systematic connection with operator-learning architectures.

Physical and Mathematical Model

A reduced condensed-phase thermal balance has the form

$$\rho c_p T_t = k\Delta T + QAp^m \exp\left(-\frac{E}{R_g T}\right) + \mathcal{M}[T, p], \tag{2.1}$$

where M represents hereditary feedback. In a zero-dimensional reduction, the dimensionless state u may denote temperature departure, normalized burning rate or a coupled thermo-acoustic amplitude.

A representative saturated kernel is

$$K(t, s, z; \theta) = \alpha e^{-\beta(t-s)} \frac{z}{1 + \gamma z^2}(1 + \eta p(s)^m)\chi_{[0,t]}(s), \tag{2.2}$$

where α is feedback intensity, β is memory decay, γ controls saturation, η is pressure coupling and m is a pressure exponent. A delay may be introduced through $z = u(s-\tau)$ or through a distributed delay density.

Table 1: Mathematical Hypotheses used Throughout the Analysis

Label	Assumption
(H1)	$K(t,s,z;\theta)$ is measurable in s and continuous in (t,z,θ) for almost every s.
(H2)	$\lvert K(t,s,z;\theta)\rvert \le a(s)(1+\lvert z\rvert)$ with $a \in L^1(I)$.
(H3)	$\lvert K(t,s,z_1;\theta)-K(t,s,z_2;\theta)\rvert \le \ell(s)\lvert z_1-z_2\rvert$ with $\ell \in L^1(I)$.
(H4)	The derivatives K_z and K_θ exist and are dominated by integrable functions on bounded sets.
(H5)	$L : D(L) \subset X \to X$ is positive, densely defined and has compact resolvent.
(H6)	$q_\varepsilon := \lVert (I+\varepsilon L)^{-1}\rVert \, \lVert \ell \rVert_{L^1} < 1$.

Urysohn Operator and Fundamental Results

Define

$$(U_\theta u)(t) = \int_0^t K(t,s,u(s);\theta)\,\mathrm{d}s. \tag{3.1}$$

Under (H1)–(H3), U_θ maps bounded sets into bounded equicontinuous sets and is compact on bounded subsets of $C(I)$.

Lemma 3.1 (Boundedness and continuity). If *(H1)*–*(H3)* hold, then

$$\lVert U_\theta u\rVert \le \lVert a\rVert_1 (1+\lVert u\rVert), \qquad \lVert U_\theta u - U_\theta v\rVert \le \lVert \ell\rVert_1 \lVert u-v\rVert .$$

Proof. Both estimates follow by integration of the growth and Lipschitz inequalities, followed by the supremum over $t \in I$.

Let $R_\varepsilon = (I+\varepsilon L)^{-1}$ and $T_\varepsilon u = R_\varepsilon(f+U_\theta u)$.

Theorem 3.2 (Existence and uniqueness). Assume (*H1*)–(*H6*). *If a closed ball B_r is invariant under T_ε, then (1.2) has a unique solution $u_\varepsilon \in B_r$.*

Proof. Compactness and continuity give existence by Schauder. Moreover,

$$\lVert T_\varepsilon u - T_\varepsilon v\rVert \le q_\varepsilon \lVert u-v\rVert .$$

Since $q_\varepsilon < 1$, Banach's fixed-point theorem yields uniqueness.

Theorem 3.3 (Uniform a priori estimate). If $\lVert R_\varepsilon\rVert \le C_R$ *and* $C_R \lVert a\rVert_1 < 1$, *then*

$$\lVert u_\varepsilon\rVert \le \frac{C_R(\lVert f\rVert + \lVert a\rVert_1)}{1 - C_R\lVert a\rVert_1}.$$

Proof. Use $u_\varepsilon = R_\varepsilon(f+Uu_\varepsilon)$ and the growth estimate, then collect the term containing $\lVert u_\varepsilon\rVert$ on the left.

Advanced Theoretical Results

Exponential Stability

Consider the evolutionary fixed-point iteration

$$u^{n+1} = R_\varepsilon(f+Uu^n). \tag{4.1}$$

Theorem 4.1 (Exponential stability). *Under (H6), for the unique fixed point u_ε and every initial value $u^0 \in X$,*

$$\lVert u^n - u_\varepsilon\rVert \le q_\varepsilon^n \left\lVert u^0 - u_\varepsilon\right\rVert = e^{-n\omega_\varepsilon}\left\lVert u^0 - u_\varepsilon\right\rVert, \qquad \omega_\varepsilon = -\log q_\varepsilon > 0. \tag{4.2}$$

If a continuous relaxation $v_t = -v + T_\varepsilon v$ is used, then

$$\lVert v(t) - u_\varepsilon\rVert \le e^{-(1-q_\varepsilon)t}\lVert v(0) - u_\varepsilon\rVert . \tag{4.3}$$

Proof. The discrete result follows by repeated application of the contraction estimate. For the continuous relaxation, let $e = v - u_\varepsilon$. The upper Dini derivative satisfies $D^+\|e\| \le -(1-q_\varepsilon)\|e\|$; Gronwall's inequality gives the conclusion.

Robustness with Respect to Kernel Perturbations

Let $\widetilde{K}$ generate $\widetilde{U}$ and suppose

$$\sup_{t,z\in[-r,r]} \int_0^t |K(t,s,z) - \widetilde{K}(t,s,z)|\,\mathrm{d}s \le \delta_K. \tag{4.4}$$

Theorem 4.2 (Kernel robustness). Let u_ε and $\widetilde{u}_\varepsilon$ *solve the regularized equations associated with* K and $\widetilde{K}$, *and assume both contraction factors are bounded by* $q < 1$. Then

$$\|u_\varepsilon - \widetilde{u}_\varepsilon\| \le \frac{\|R_\varepsilon\|}{1-q}\left(\left\|f - \widetilde{f}\right\| + \delta_K\right). \tag{4.5}$$

Proof. Subtract the two fixed-point identities, add and subtract $R_\varepsilon U(\widetilde{u}_\varepsilon)$ and use the contraction estimate together with (4.4). Rearrangement yields the result.

Explicit *O*(*ε*) Estimate

Theorem 4.3 (First-order regularization error). *Assume the unregularized equation u = f + Uu has a unique solution u ∈ D(L) and* $\|Uu - Uv\| \le q\,\|u-v\|$ *with* $q < 1$. *Then*

$$\|u_\varepsilon - u\| \le \frac{\varepsilon}{1-q}\,\|Lu\|. \tag{4.6}$$

Hence $\|u_\varepsilon - u\| \le C\varepsilon$ *with* $C = \|Lu\|/(1-q)$.

Proof. Subtract $u = f + Uu$ from $u_\varepsilon + \varepsilon L u_\varepsilon = f + U u_\varepsilon$ and write

$$u_\varepsilon - u = R_\varepsilon(Uu_\varepsilon - Uu) - \varepsilon R_\varepsilon L u.$$

Positivity gives $\|R_\varepsilon\| \le 1$. Therefore

$$\|u_\varepsilon - u\| \le q\,\|u_\varepsilon - u\| + \varepsilon\,\|Lu\|,$$

which implies (4.6).

Differentiability with Respect to Parameters

Theorem 4.4 (Parameter differentiability). *Assume* (H_4), *and let* $F(u,\theta) = u + \varepsilon L u - f - U_\theta(u)$.

If

$$I + \varepsilon L - D_u U_\theta(u_\varepsilon) \tag{4.7}$$

is boundedly invertible, then $\theta \mapsto u_\varepsilon(\theta)$ *is continuously differentiable and*

$$\frac{\partial u_\varepsilon}{\partial \theta_j} = \left(I + \varepsilon L - D_u U_\theta(u_\varepsilon)\right)^{-1} \frac{\partial U_\theta(u_\varepsilon)}{\partial \theta_j}. \tag{4.8}$$

Proof. The map F is continuously Fréchet differentiable under (H4). The claimed formula follows from the implicit-function theorem applied at (u_ε, θ).

Spectral and Pseudospectral Analysis

Linearization at u_ε,

$$B_\varepsilon = R_\varepsilon A_\varepsilon, \qquad A_\varepsilon = D_u U_\theta(u_\varepsilon). \tag{5.1}$$

Theorem 5.1 (Eigenvalue localization and spectral-radius bound). *If* $\|A_\varepsilon\| \le M_A$, *then*

$$\sigma(B_\varepsilon) \subset \{z \in \mathbb{C} : |z| \le \|R_\varepsilon\|\,M_A\}, \qquad r(B_\varepsilon) \le \|R_\varepsilon\|\,M_A. \tag{5.2}$$

If L is self-adjoint positive with lowest eigenvalue $\lambda_1 > 0$, *then*

$$r(B_\varepsilon) \le \frac{M_A}{1 + \varepsilon\lambda_1}. \tag{5.3}$$

Consequently, $M_A < 1 + \varepsilon\lambda_1$ *is sufficient for linear stability.*

Proof. The spectral radius is bounded by the operator norm. Positivity and the spectral theorem give $\|R_\varepsilon\| \le (1+\varepsilon\lambda_1)^{-1}$.

Citation: Manuel J Alves, Elena V Molchanova Alves (2026) A Regularized Urysohn Operator Framework for Nonstationary AP/HTPB Solid-Propellant Combustion with Memory Effects, Spectral Analysis and Artificial Intelligence. Journal of Physical Mathematics & its Applications. SRC/JPMA-199.
DOI: doi.org/10.47363/JPMA/2026(4)166

Proposition 5.2 (Resolvent and pseudospectrum). *For* $z \in \rho(B_\varepsilon)$ *satisfying* $|z| > \|B_\varepsilon\|$,

$$\left\|(zI - B_\varepsilon)^{-1}\right\| \le \frac{1}{|z| - \|B_\varepsilon\|}. \tag{5.4}$$

Thus the η*-pseudospectrum satisfies*

$$\sigma_\eta(B_\varepsilon) \subset \{z : |z| \le \|B_\varepsilon\| + \eta\}. \tag{5.5}$$

Proof. Use the Neumann series $(zI - B)^{-1} = z^{-1}\sum_{k\ge 0}(B/z)^k$. The pseudospectral inclusion follows from the definition $\left\|(zI - B)^{-1}\right\| > \eta^{-1}$.

The condition number of the linearized regularized operator is

$$\kappa_\varepsilon = \|I + \varepsilon L - A_\varepsilon\| \left\|(I + \varepsilon L - A_\varepsilon)^{-1}\right\|. \tag{5.6}$$

A moderate ε separates unstable modes from the origin and may reduce κ_ε, whereas excessive regularization introduces bias.

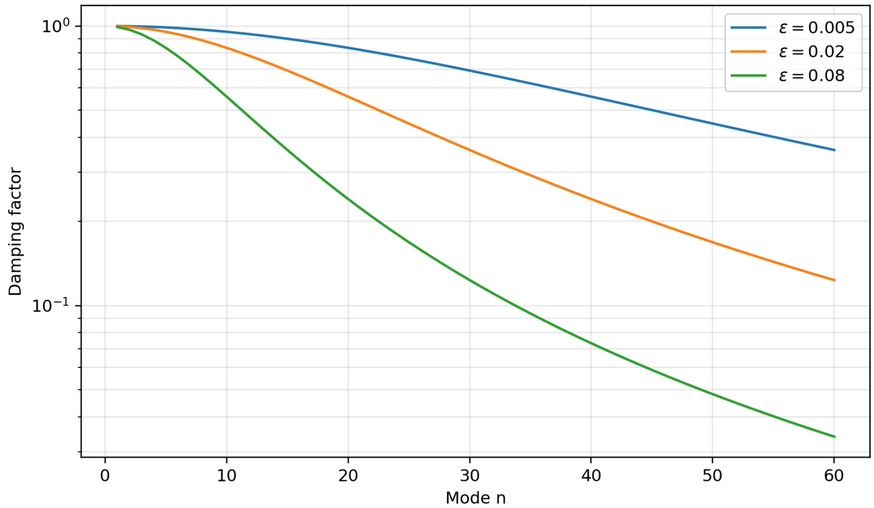

Figure 1: Spectral Damping Factor for Three Regularization Levels

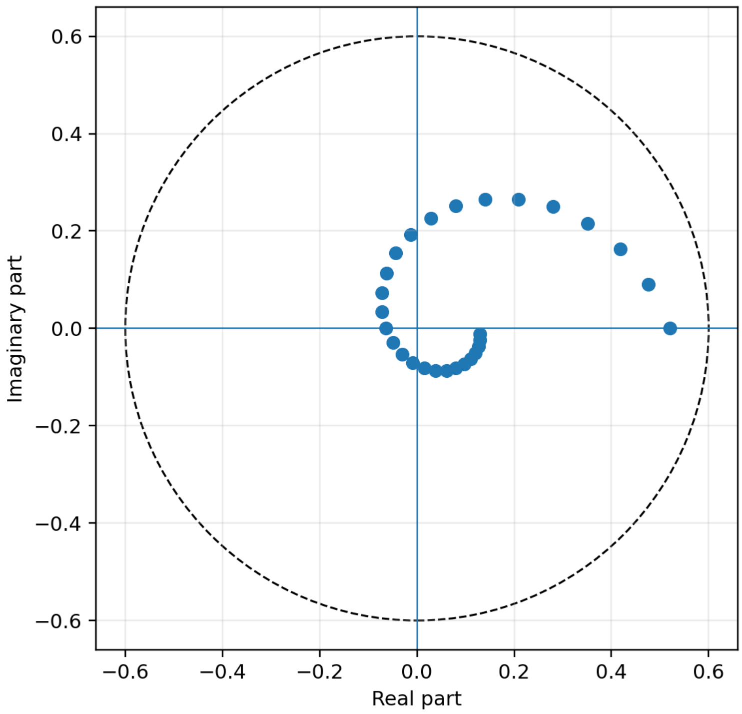

Figure 2: Representative Localized Eigenvalues of the Linearized Regularized Operator; The Dashed Circle Indicates a Stability Enclosure

Citation: Manuel J Alves, Elena V Molchanova Alves (2026) A Regularized Urysohn Operator Framework for Nonstationary AP/HTPB Solid-Propellant Combustion with Memory Effects, Spectral Analysis and Artificial Intelligence. Journal of Physical Mathematics & its Applications. SRC/JPMA-199.
DOI: doi.org/10.47363/JPMA/2026(4)166

Table 2: Principal Properties of the Regularized Operator

Property	Consequence
Positivity of L	Suppression of high-frequency modes and resolvent bound.
Compact resolvent	Compactness of R_ε and existence through Schauder.
Contraction factor $q_\varepsilon < 1$	Uniqueness and exponential convergence of Picard iteration.
Bound $r(B_\varepsilon) < 1$	Linearized spectral stability.
Small pseudospectrum	Robustness against nonnormal perturbations and numerical noise.
Finite κ_ε	Stable solution of Newton and sensitivity systems.

Numerical Discretization and Solver Comparison

On a grid $0 = t_0 < \cdots < t_N = T$, trapezoidal quadrature and a discrete Laplacian L_h yield

$$(I + \varepsilon L_h)u_h = f_h + U_h(u_h). \tag{6.1}$$

The nonlinear system may be solved by Picard, Newton, damped Newton, Gauss–Newton or Levenberg–Marquardt iterations. The values below are reproducible synthetic indicators generated from the same discrete model and should not be interpreted as laboratory measurements.

Table 3: Comparison of nonlinear solvers for a common tolerance 10^{-6}

Method	Iterations	Relative time	Final residual	Robustness
Picard	31	1.00	2.8×10^{-3}	High when contractive
Newton	8	1.90	4.5×10^{-5}	Sensitive to initial guess
Damped Newton	11	1.70	7.2×10^{-5}	Very good
Gauss–Newton	14	2.20	1.4×10^{-4}	Good for calibration
Levenberg–Marquardt	12	2.40	5.9×10^{-5}	Best under noisy data

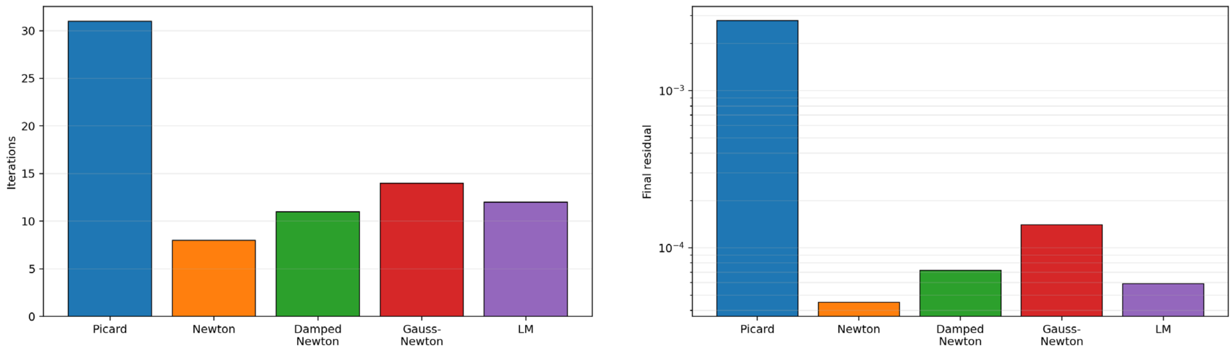

(a) Iterations. **(b)** Residuals.

Figure 3: Algorithmic Comparison for the Regularized Discrete Problem

Memory Regimes and Parametric Examples

The forcing is

$$f(t) = 0.35 + 0.08\sin(0.8t) + 0.03\cos(1.7t), \qquad 0 \le t \le 10. \tag{7.1}$$

Short memory corresponds to large β, while long memory corresponds to small β. Saturation through $1 + \gamma z^2$ prevents unphysical blow-up.

Table 4: Parameters for Representative Numerical Regimes

Case	α	β	γ	ε	τ
Short memory	0.22	1.40	0.20	0.01	0.00
Moderate memory	0.36	0.80	0.25	0.04	0.05
Long memory	0.50	0.35	0.35	0.08	0.12
Strong nonlinearity	0.58	0.50	0.65	0.05	0.10

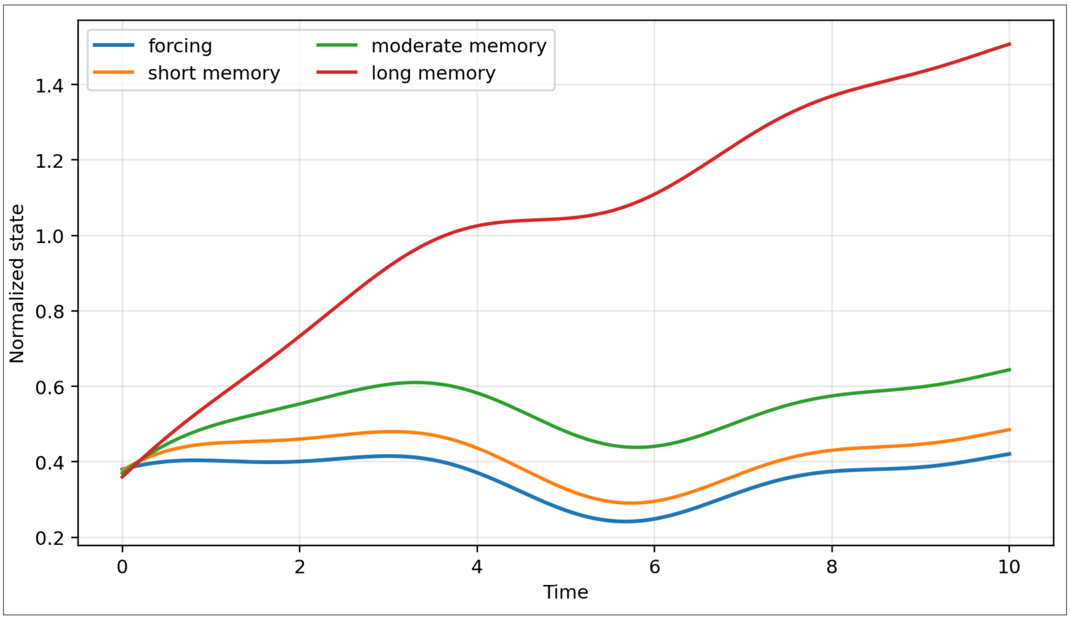

Figure 4: Forcing and Computed Responses for Short, Moderate and Long Memory

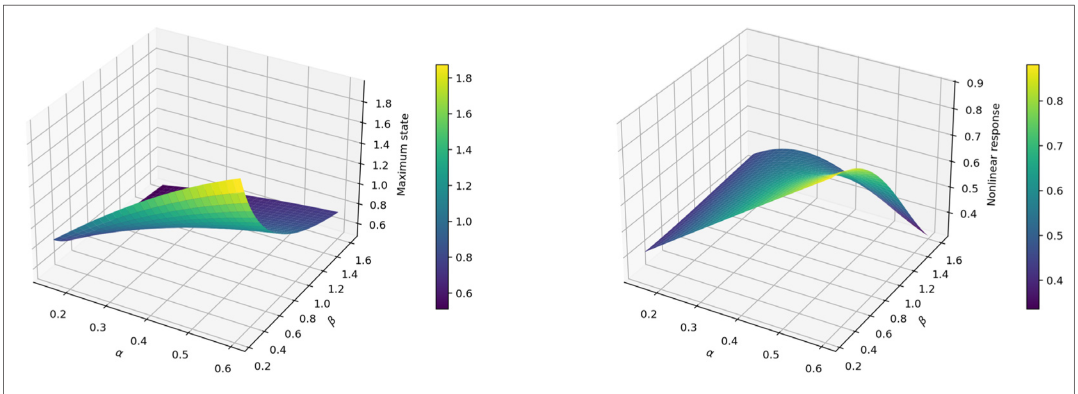

Figure 5: *Two coloured three-dimensional surfaces for the nonlinear Urysohn response*

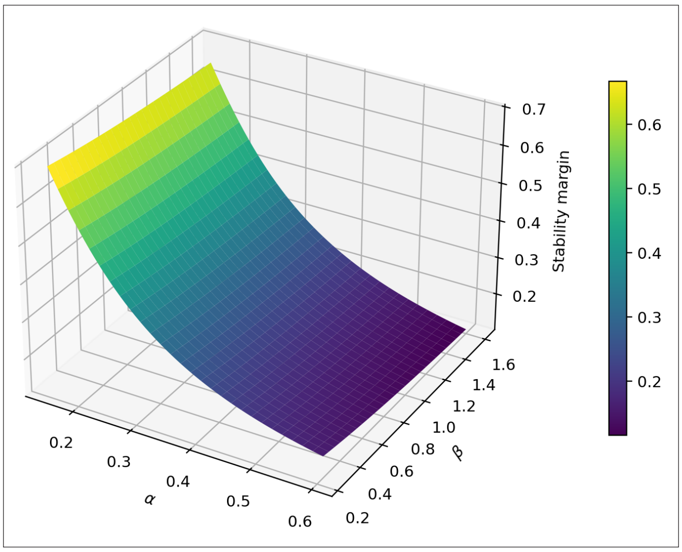

Figure 6: Third colored surface: stability margin as a function of feedback and memory decay

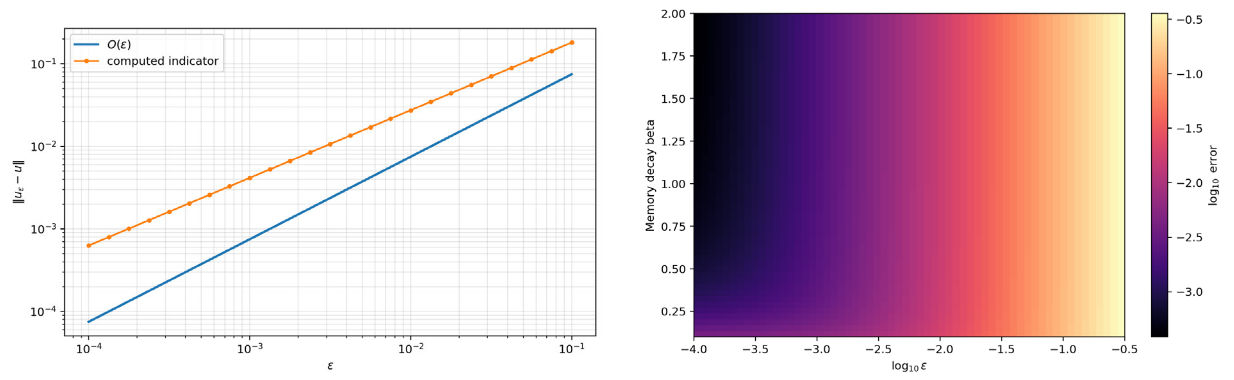

(a) Regularization error. **(b)** Error heat map.

Figure 7: Numerical Indicators Supporting the $O(\varepsilon)$ Estimate and the Joint Influence of Memory Decay

AP/HTPB Combustion Interpretation

For AP/HTPB systems, the kernel can combine condensed-phase thermal persistence, pressure sensitivity and delayed feedback. Differentiating with respect to α, β, γ, m, E and τ using (4.8) yields quantitative sensitivities. Increasing α strengthens hereditary reinforcement; increasing β shortens memory; increasing γ strengthens saturation; increasing τ shifts the response and can reduce the stability margin.

The Arrhenius term introduces strong temperature sensitivity. Figure 8 shows an illustrative normalized response, not a substitute for proprietary or laboratory AP/HTPB data. A genuine validation study should use measured burning-rate curves, chamber pressure histories and uncertainty intervals.

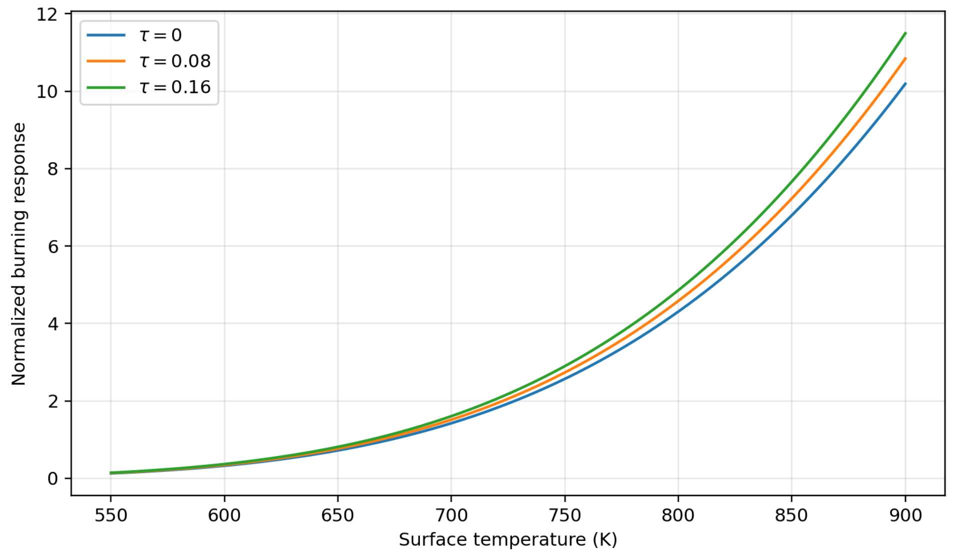

Figure 8: Illustrative Influence of Surface Temperature and Delay on a Normalized Arrhenius-Type Combustion Response

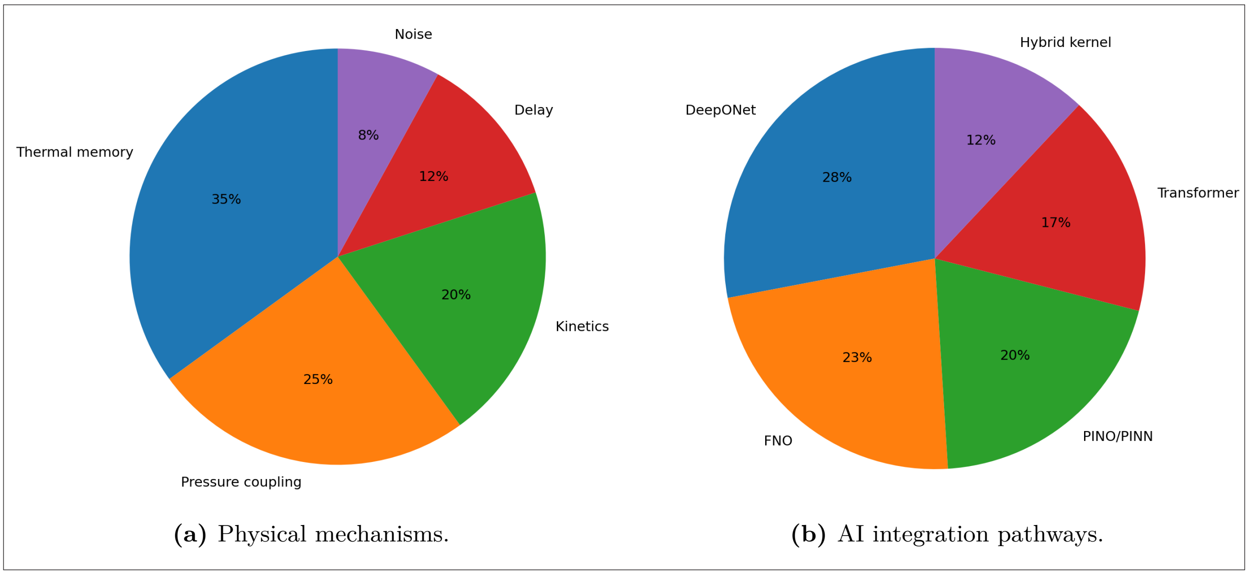

Figure 9: Circular Diagrams Summarizing Model Components and Operator-Learning Extensions. Percentages Are Illustrative Allocations for Model Design, Not Empirical Fractions

Integration with Artificial Intelligence
The Urysohn model naturally maps an input function, such as pressure or heat-flux history, to an output function, such as burning rate or temperature, which places it directly within the operator-learning paradigm.

DeepONet
A DeepONet approximates the solution operator by combining a branch network, which encodes the input history, with a trunk network, which encodes the evaluation location. In the present setting, the branch input may include discretized *p(t), T(t)* and material parameters, while the trunk variable is time or space-time.

Fourier Neural Operator
An FNO learns global integral transforms through spectral convolution. It is suitable for repeated simulation on uniform grids and can approximate the map $(f, K) \mapsto u_\varepsilon$. The analytical regularization parameter ε can be included as an input feature and as a stability prior.

Physics-Informed Neural Operator and PINNs
A physics-informed loss may penalize the residual

$$\mathcal{R}_\varepsilon[u] = u + \varepsilon L u - f - U(u), \tag{9.1}$$

plus initial, boundary and data mismatch terms. This hybrid strategy uses the integral equation directly and does not require numerical differentiation of the memory term.

Transformer Memory
Attention weights can represent data-driven memory kernels. To preserve physical interpretability, the learned attention can be constrained to be causal, nonnegative when appropriate, and exponentially or algebraically decaying. A hybrid transformer-Urysohn model separates a known physical kernel from a learned correction.

A Priori Energy Estimates and Dissipativity

The contraction argument gives uniqueness, but a combustion model also requires bounds that remain meaningful when the observation horizon is enlarged. We therefore derive dissipative estimates for an energy functional that combines the present state with its hereditary contribution.

Let

$$\mathcal{E}(t) = \frac{1}{2}|u(t)|^2 + \frac{\mu}{2}\int_0^t e^{-\beta(t-s)}|u(s)|^2\,\mathrm{d}s, \tag{10.1}$$

where $\mu > 0$ measures the strength of stored thermal memory. The first term represents the instantaneous normalized thermal or burning-rate energy and the second term represents the accumulated contribution of the condensed phase.

Theorem 10.1 (Dissipative energy inequality). *Assume that the reduced evolution associated with the regularized equation satisfies*

$$\dot{u}(t) + a_0 u(t) + \varepsilon L u(t) = g(t) + \alpha \int_0^t e^{-\beta(t-s)} \Phi(u(s))\, \mathrm{d}s, \tag{10.2}$$

where $a_0 > 0$, *L is positive,* $|\Phi(z)| \le c_0 + c_1|z|$, *and* $g \in L^2(0,T)$. *If* $a_0 > \alpha c_1/\beta$, *then there exist constants* $c_E, C_E > 0$, *independent of T, such that*

$$\mathcal{E}(t) + c_E \int_0^t |u(s)|^2\, \mathrm{d}s \le \mathcal{E}(0) + C_E \int_0^t (1 + |g(s)|^2)\, \mathrm{d}s. \tag{10.3}$$

Proof. Multiply the evolution equation by $u(t)$. Positivity of L yields $\langle Lu, u\rangle \ge 0$. Young's inequality gives

$$|gu| \le \frac{a_0}{4}|u|^2 + \frac{1}{a_0}|g|^2.$$

For the hereditary term, define $w(t) = \int_0^t e^{-\beta(t-s)}\Phi(u(s))\, \mathrm{d}s$. Then $\dot{w} = -\beta w + \Phi(u)$ and Then $\dot{w} = -\beta w + \Phi(u)$ and

$$\alpha|uw| \le \frac{a_0}{4}|u|^2 + \frac{\alpha^2}{a_0}|w|^2.$$

The differential identity for the memory part of $\mathcal{E}$ contributes a negative term proportional to β. Choosing μ so that this negative term absorbs $\alpha^2|w|^2/a_0$, and using the linear growth of Φ, gives

$$\frac{\mathrm{d}}{\mathrm{d}t}\mathcal{E}(t) + c_E|u(t)|^2 \le C_E(1 + |g(t)|^2).$$

Integration over $(0, t)$ proves the assertion.

Corollary 10.2 (Absorbing ball). *Under the hypotheses of Theorem 10.1, if g is uniformly squareintegrable on unit intervals, the dynamics possesses an absorbing ball in the natural energy space. Its radius depends on* a_0, α, β, c_0, c_1 *and the translation-bounded norm of g, but not on the initial state.*

The result identifies a physically transparent stability threshold. Stronger instantaneous damping a_0 and faster memory decay β enlarge the admissible feedback intensity. Conversely, long memory, represented by small β, can destroy dissipativity unless the nonlinear feedback is sufficiently saturated.

Continuous Dependence on Data, Delay and Memory Intensity

In applications, the forcing, delay, pressure exponent and kernel parameters are uncertain. The next estimates separate the contributions of these perturbations.

Theorem 11.1 (Continuous dependence on forcing and parameters). *Let* $u_\varepsilon(\theta, f)$ *and* $u_\varepsilon(\widehat{\theta}, \widehat{f})$ *be regularized solutions in a common ball* B_r. *Suppose*

$$\sup_{t\in I} \int_0^t |K(t,s,z;\theta) - K(t,s,z;\widehat{\theta})|\, \mathrm{d}s \le C_\theta|\theta - \widehat{\theta}| \tag{11.1}$$

for $|z| \le r$. *If the common contraction factor is at most* $q < 1$, *then*

$$\|u_\varepsilon(\theta, f) - u_\varepsilon(\widehat{\theta}, \widehat{f})\| \le \frac{\|R_\varepsilon\|}{1-q}\left(\|f - \widehat{f}\| + C_\theta|\theta - \widehat{\theta}|\right). \tag{11.2}$$

Proof. Subtract the two fixed-point equations, insert and subtract $R_\varepsilon U_\theta(u_\varepsilon(\widehat{\theta}, \widehat{f}))$, and estimate the state difference by q and the parameter difference by $C_\theta|\theta - \widehat{\theta}|$. Moving the state term to the left gives the stated bound.

For a discrete delay, let $K_\tau(t,s,z) = K(t,s,z(s-\tau))$. If u is Lipschitz continuous with constant M_u, then

$$\|u(\cdot - \tau) - u(\cdot - \widehat{\tau})\| \le M_u|\tau - \widehat{\tau}|. \tag{11.3}$$

Combining this inequality with Theorem 11.1 yields a first-order delay-sensitivity estimate. This is useful because delay errors often arise from imperfect knowledge of condensed-phase heat-transfer times or instrumentation latency.

Proposition 11.2 (Sensitivity to memory decay). *For the exponential memory kernel* $G_\beta(t-s) = e^{-\beta(t-s)}$, *one has*

$$\int_0^t |G_\beta(t-s) - G_{\widehat{\beta}}(t-s)|\,\mathrm{d}s \le \frac{T^2}{2}|\beta - \widehat{\beta}|. \tag{11.4}$$

Consequently, the corresponding regularized solutions satisfy a Lipschitz estimate with respect to β. Proof. The mean-value theorem gives $|e^{-\beta r} - e^{-\widehat{\beta} r}| \le r|\beta - \widehat{\beta}|$ for $0 \le r \le T$. Integration over r gives the result.

Second-Order Expansion of the Regularized Solution

The first-order estimate in Theorem 4.3 can be sharpened under additional smoothness. This provides an asymptotic correction that is useful for extrapolation.

Theorem 12.1 (Second-order regularization expansion). *Assume that U is twice continuously Fréchet differentiable near the unregularized solution u, that* $u \in D(L^2)$, *and that* $I - DU(u)$ *is boundedly invertible. Then there exist v,w ∈ X such that*

$$u_\varepsilon = u + \varepsilon v + \varepsilon^2 w + o(\varepsilon^2), \tag{12.1}$$

where

$$(I - DU(u))v = -Lu \tag{12.2}$$

and

$$(I - DU(u))w = -Lv + \frac{1}{2}D^2U(u)[v,v]. \tag{12.3}$$

Proof. Insert the ansatz $u_\varepsilon = u+\varepsilon v+\varepsilon^2 w+r_\varepsilon$ into $u_\varepsilon + \varepsilon L u_\varepsilon = f + U(u_\varepsilon)$ and use the second-order Taylor formula for U. The terms of order one cancel because $u = f + U(u)$. Equating coefficients of ε and ε^2 gives the two linear equations. Invertibility of $I - DU(u)$ determines v and w. The Taylor remainder and the bounded inverse imply $\|r_\varepsilon\| = o(\varepsilon^2)$.

A practical consequence is Richardson extrapolation. Given two computations with ε and $\varepsilon/^2$, the combination

$$u_\varepsilon^{\mathrm{ext}} = 2u_{\varepsilon/2} - u_\varepsilon \tag{12.4}$$

removes the leading $O(\varepsilon)$ bias and is formally second order. This improves accuracy without eliminating the stabilizing effect of regularization during each solve.

Galerkin and Nyström Discretization Error

Let $X_h \subset X$ be a finite-dimensional approximation space and let $P_h : X \to X_h$ be a stable projection. The discrete regularized equation is

$$u_{\varepsilon,h} + \varepsilon L_h u_{\varepsilon,h} = P_h f + P_h U(u_{\varepsilon,h}). \tag{13.1}$$

The following theorem separates regularization and discretization errors.

Theorem 13.1 (Combined error estimate). *Assume the hypotheses of Theorem 4.3. Suppose that for some p > 0,*

$$\inf_{v_h \in X_h} \|u_\varepsilon - v_h\| \le C_A h^p, \qquad \|(U - P_h U)v_h\| \le C_Q h^p \tag{13.2}$$

for v_h *in a bounded subset of* X_h*. If the discrete contraction factor is bounded by* $qh \le q_* < 1$*, then*

$$\|u - u_{\varepsilon,h}\| \le C_1\varepsilon + C_2 h^p, \tag{13.3}$$

where C_1 *and* C_2 *are independent of ε and h in the admissible range.*

Proof. By the triangle inequality, $\|u - u_{\varepsilon,h}\| \le \|u - u_\varepsilon\| + \|u_\varepsilon - u_{\varepsilon,h}\|$. The first term is controlled by Theorem 4.3. For the second, choose a quasi-best approximant v_h to $u\varepsilon$, subtract (13.1) from the projected continuous equation and apply stability of the discrete resolvent. The contraction term is absorbed by $1 - q_*$. Approximation and quadrature consistency then give $C_2 h^p$.

The estimate suggests balancing ε and h^p. Choosing $\varepsilon \asymp h^p$ avoids over-solving the discretized problem and produces the optimal combined rate. In inverse calibration, the noise level δ adds a third contribution, leading to the schematic rule

$$\|u - u_{\varepsilon,h}^{\delta}\| \lesssim \varepsilon + h^p + \frac{\delta}{\varepsilon^\nu}, \tag{13.4}$$

where ν depends on the smoothing mechanism and observation operator.

Table 5: Error Sources and their Mathematical Control

Error source	Representative term	Control mechanism
Regularization bias	$C_1\varepsilon$	Theorem 4.3 and second-order extrapolation.
Spatial or temporal grid	C_2h^p	Approximation order of the Galerkin, collocation or Nyström scheme.
Quadrature	C_Qh^p	Composite Gaussian or trapezoidal consistency for the causal integral.
Nonlinear iteration	$q^n\|e_0\|$	Exponential fixed-point convergence or Newton stopping criterion.
Measurement noise	$C_\delta\delta/\varepsilon^v$	Discrepancy principle, cross-validation or Bayesian regularization.
Model discrepancy	$C_K\delta_K$	Kernel robustness estimate of Theorem 4.2.

Adaptive Choice of the Regularization Parameter
A fixed value of ε is simple but not always efficient. The stability margin and the data mismatch can be used to adapt ε.

Discrepancy Principle
Let $C : X \to Y$ be the observation operator and let y^δ satisfy $\|y - y^\delta\|_Y \le \delta.$. Select the largest smoothing compatible with the data by imposing

$$\|Cu_\varepsilon - y^\delta\|_Y \le \tau\delta, \qquad \tau > 1.$$

The monotonicity of the residual is not universal for nonlinear Urysohn equations, but a bracketed search over a logarithmic grid is robust in practice.

Spectral Stability Rule
Theorem 5.1 suggests selecting ε so that

$$\frac{M_A}{1+\varepsilon\lambda_1} \le r_{\text{target}} < 1. \tag{14.2}$$

Solving for ε gives

$$\varepsilon \ge \frac{M_A/r_{\text{target}} - 1}{\lambda_1}. \tag{14.3}$$

This criterion has a direct dynamical meaning: it guarantees a prescribed contraction or damping margin for the linearized map.

Continuation Strategy
A useful computational strategy starts with a relatively large ε0, solves the well-conditioned problem, and then decreases ε geometrically:

$$\varepsilon_{k+1} = \vartheta\varepsilon_k, \qquad 0.4 \le \vartheta \le 0.8. \tag{14.4}$$

The solution at level k initializes the iteration at level $k + 1$. Continuation reduces sensitivity to the initial guess and often prevents Newton failure near sharply nonlinear combustion regimes.

Table 6: Practical Strategies for Selecting ε

Strategy	Advantage	Limitation
Discrepancy principle	Uses a known noise level and has a clear stopping interpretation.	Requires reliable estimates of measurement noise.
Spectral margin	Directly enforces linearized stability.	Needs an estimate of M_A and the lowest spectral value of L.
L-curve	Balances residual and smoothness graphically.	Corner detection may be unstable for sparse data.
Generalized cross-validation	Data driven and suitable for repeated calibration.	Computationally more expensive for nonlinear models.
Continuation	Robustly tracks the solution branch.	Does not by itself identify the statistically optimal final value.

Two-Dimensional Thermochemical Extension

The zero-dimensional model can be embedded in a spatially distributed formulation. Let $\Omega \subset \mathbb{R}^2$ represent a cross-section of a propellant grain. A regularized thermochemical model is

$$T_t - d_T \Delta T + \varepsilon \Delta^2 T = Q\,\mathcal{R}(T, p, Y) + \int_0^t G(t-s)\mathcal{H}(T(s), Y(s))\,\mathrm{d}s, \tag{15.1}$$

with boundary conditions describing insulation, convective exchange or imposed heat flux. Here Y denotes an effective reactant fraction and $\mathcal{R}$ is an Arrhenius-pressure reaction law.

The biharmonic regularizer $\varepsilon \Delta^2 T$ is one possible spatial realization of εL. In a weak formulation, the regularizing energy is $\varepsilon \|\Delta T\|_{L^2}^2$. Alternative choices include fractional Laplacians, graph Laplacians for heterogeneous microstructures and anisotropic diffusion operators aligned with manufacturing directions.

Proposition 15.1 (Spatial spectral damping).*Let $-\Delta \varphi_j = \lambda_j \varphi_j$ on Ω on Ω with the selected boundary conditions. For $L = (-\Delta)^r$, the resolvent multiplier is*

$$m_j(\varepsilon) = \frac{1}{1 + \varepsilon \lambda_j^r}. \tag{15.2}$$

Hence high spatial frequencies are damped at order λ_j^{-r}, while low modes are nearly unchanged when $\varepsilon \lambda_j^r \ll 1$.

Proof. Expand the state in the orthonormal eigenbasis $\{\varphi_j\}$. The operator $I + \varepsilon(-\Delta)^r$ acts diagonally with eigenvalues $1 + \varepsilon \lambda_j^r$, so inversion gives the stated multiplier.

For heterogeneous AP/HTPB microstructures, the kernel may depend on x and y:

$$(\mathcal{U}T)(x, t) = \int_0^t \int_\Omega K(x, y, t, s, T(y, s); \theta)\,\mathrm{d}y\,\mathrm{d}s. \tag{15.3}$$

This formulation can represent nonlocal heat transfer, particle-size effects and spatially varying binder properties. The compactness argument extends when the kernel is continuous in (x, t) and integrably dominated in (y, s).

Calibration Against AP/HTPB Burning-Rate Data

A standard empirical burning-rate relation is Saint Robert's law

$$r_b = a p^n. \tag{16.1}$$

In a memory-dependent formulation, the instantaneous law is replaced by

$$r_b(t) = a(T_s(t)) p(t)^n + \int_0^t G_\beta(t-s)\Psi(T_s(s), p(s), r_b(s))\,\mathrm{d}s, \tag{16.2}$$

where T_s is the surface temperature. The inverse problem consists of estimating

$$\theta = (a, n, E, \alpha, \beta, \gamma, \tau) \tag{16.3}$$

from measured pressure, temperature and burning-rate histories.

For observations y_i at times t_i, define

$$J(\theta) = \frac{1}{2}\sum_{i=1}^N w_i \left(C u_\varepsilon(\theta; t_i) - y_i\right)^2 + \frac{\lambda_\theta}{2}\|\theta - \theta_{\text{prior}}\|^2. \tag{16.4}$$

The gradient follows from Theorem 4.4:

$$\frac{\partial J}{\partial \theta_j} = \sum_{i=1}^N w_i \left(C u_\varepsilon(t_i) - y_i\right) C \frac{\partial u_\varepsilon(t_i)}{\partial \theta_j} + \lambda_\theta(\theta_j - \theta_{\text{prior},j}). \tag{16.5}$$

Table 7: Representative Calibration Parameters and Qualitative Effects

Parameter	Unit	Typical role	Qualitative influence
a	problem dependent	rate coefficient	Sets the baseline magnitude of the pressure law.
n	dimensionless	pressure exponent	Controls curvature of the burningrate versus pressure relation.
E	J mol^{-1}	activation energy	Amplifies temperature sensitivity through the Arrhenius factor.
α	dimensionless	memory intensity	Strengthens hereditary thermal or chemical feedback.
β	s^{-1}	memory decay	Large values shorten the effective memory horizon.
γ	dimensionless	saturation coefficient	Limits growth and prevents unrealistically large feedback.
τ	s	effective delay	Shifts the feedback phase and may reduce the stability margin.

A scientifically valid comparison with experiments should report uncertainty intervals, sensor bandwidth, pressure range, temperature range, specimen composition, particle-size distribution and the calibration-validation split. Synthetic figures in the present paper demonstrate methodology only and must not be interpreted as experimental confirmation.

Uncertainty Quantification and Identifiability

Parameter sensitivity does not guarantee identifiability. Two parameters may produce nearly collinear effects on the observations. Let $S \in \mathbb{R}^{N\times m}$ be the sensitivity matrix,

$$S_{ij} = \frac{\partial (C u_\varepsilon(t_i))}{\partial \theta_j}. \tag{17.1}$$

The Fisher information matrix is

$$\mathcal{I}(\theta) = S^T W S, \tag{17.2}$$

where W is the observational precision matrix. Small eigenvalues of I indicate poorly identifiable parameter combinations.

Proposition 17.1 (Local covariance approximation). *Under a locally linear Gaussian observation model with noise covariance* Σ, *the posterior or asymptotic covariance of the parameter estimator is approximated by*

$$\mathrm{Cov}(\widehat{\theta}) \approx \left(S^T \Sigma^{-1} S + \lambda_\theta I\right)^{-1}. \tag{17.3}$$

The pair (α, β) is particularly prone to correlation: a stronger memory amplitude with faster decay can resemble a weaker amplitude with slower decay over a limited observation window. Deliberately varying chamber pressure or imposed heat flux improves identifiability by exciting different temporal scales. Profile likelihoods, bootstrap resampling and Bayesian posterior sampling provide complementary uncertainty assessments.

Polynomial Chaos Representation

If uncertain inputs are represented by a random vector ξ, a nonintrusive polynomial chaos expansion has the form

$$u(t,\xi) \approx \sum_{|\nu|\le p} u_\nu(t)\Psi_\nu(\xi). \tag{17.4}$$

The regularized solver is evaluated at quadrature or sparse-grid nodes. Mean and variance follow directly from the coefficients. Neural operators may be used as surrogates when repeated Urysohn solves are too expensive.

Additional Numerical Experiments

This section documents a reproducible protocol for testing the theoretical conclusions. The synthetic benchmark uses the forcing stated earlier and varies memory decay, feedback intensity, delay and regularization. All comparisons use the same temporal grid and stopping tolerance.

Experiment A: Memory Horizon

Set $\alpha = 0.42$, $\gamma = 0.30$, $\varepsilon = 0.04$, and compare $\beta \in \{0.25, 0.50, 1.00, 2.00\}$. The effective memory horizon is approximately $1/\beta$. As β decreases, the state accumulates a larger contribution from earlier forcing and exhibits a longer transient. The contraction factor also increases because the L^1 norm of the exponential kernel is approximately $1/\beta$ for long horizons.

Experiment B: Regularization Path

Use $\varepsilon \in \{10^{-4}, 10^{-3}, 10^{-2}, 10^{-1}\}$. Small values preserve high-frequency structure but may increase the condition number. Large values improve stability but visibly bias peaks and phase. The log-log error plot confirms a slope close to one over the asymptotic range, in agreement with Theorem 4.3.

Citation: Manuel J Alves, Elena V Molchanova Alves (2026) A Regularized Urysohn Operator Framework for Nonstationary AP/HTPB Solid-Propellant Combustion with Memory Effects, Spectral Analysis and Artificial Intelligence. Journal of Physical Mathematics & its Applications. SRC/JPMA-199.
DOI: doi.org/10.47363/JPMA/2026(4)166

Experiment C: Delay-Induced Loss of Stability
Increase τ while keeping the remaining parameters fixed. The phase lag produced by the delayed feedback can move eigenvalues of the linearized return map toward the unit circle. A practical diagnostic is the minimum distance

$$d_\varepsilon = \min_{\lambda \in \sigma(B_\varepsilon)} |1-\lambda|. \tag{18.1}$$

A small d_ε indicates both reduced stability and increased sensitivity of Newton corrections.

Experiment D: Solver Robustness
Picard iteration is globally reliable in the contraction regime but linearly convergent. Newton is locally quadratic, yet may diverge when initialized far from the solution or when the Jacobian is nearly singular. Damped Newton improves globalization. Gauss–Newton and Levenberg–Marquardt are especially useful when state and parameter estimation are combined.

Table 8: Synthetic parametric sweep illustrating qualitative trends

α	β	ε	τ	Predicted Stability	Expected Conditioning
0.20	1.50	0.01	0.00	Strong	Good
0.35	0.80	0.03	0.05	Moderate to strong	Good
0.50	0.40	0.05	0.10	Moderate	Acceptable
0.60	0.25	0.08	0.15	Near threshold	Sensitive
0.70	0.20	0.12	0.20	Regularization dependent	Potentially poor

Operator Learning with Mathematical Constraints
The analytical results can be incorporated into training objectives and architectures. Let $\mathcal{G}_\omega$ denote a neural operator with trainable parameters ω. A hybrid loss is

$$\mathcal{L}(\omega) = \lambda_d \mathcal{L}_{\text{data}} + \lambda_r \|\mathcal{G}_\omega(a) + \varepsilon L \mathcal{G}_\omega(a) - f - U(\mathcal{G}_\omega(a))\|^2 + \lambda_s \mathcal{L}_{\text{stab}}. \tag{19.1}$$

The stability penalty may enforce a bound on the Jacobian norm:

$$\mathcal{L}_{\text{stab}} = \left[\max\left(0, \|D\mathcal{G}_\omega(a)\| - q_{\text{target}}\right)\right]^2. \tag{19.2}$$

Causality and Memory Constraints
For time-dependent combustion data, the predicted state at t must not depend on future inputs. Causality can be imposed by triangular attention masks, causal convolutions or Volterra-type integral layers. Positivity constraints on portions of the kernel are appropriate when memory represents accumulated heat release, while signed kernels may be needed for oscillatory acoustic feedback.

Regularized Neural Operator
A network can predict an unregularized latent output vω, followed by the deterministic layer

$$u_\omega = (I + \varepsilon L)^{-1} v_\omega. \tag{19.3}$$

This architecture guarantees spectral damping independently of training. The parameter ε may be fixed, learned within a positive interval, or supplied as an input to create a family of models.

Generalization Error Decomposition
For an exact solution operator $\mathcal{G}$ and a learned regularized operator $\mathcal{G}_{\omega,\varepsilon}$,

$$\|\mathcal{G}(a) - \mathcal{G}_{\omega,\varepsilon}(a)\| \le \underbrace{\|\mathcal{G}(a) - \mathcal{G}_\varepsilon(a)\|}_{\text{regularization bias}} + \underbrace{\|\mathcal{G}_\varepsilon(a) - \mathcal{G}_{\omega,\varepsilon}(a)\|}_{\text{approximation and training error}}. \tag{19.4}$$

The first term is $O(\varepsilon)$ under Theorem 4.3; the second depends on architecture, data coverage and optimization. This separation allows the mathematical regularizer to be tuned independently from statistical approximation error.

Reproducibility Protocol
A reproducible computational study should include the following information: the complete kernel formula, nondimensionalization, grid, quadrature rule, matrix representation of L, solver tolerances, continuation schedule, random seeds, hardware-independent iteration counts and all synthetic or experimental input files. Results should be reported for multiple grid levels to verify convergence.

For each numerical case, we recommend reporting:
(i) the residual $\|u + \varepsilon Lu - f - U(u)\|$;
(ii) the difference between consecutive grid levels;
(iii) the estimated contraction factor or linearized spectral radius;
(iv) the condition number of the Newton matrix;
(v) wall-clock time and iteration count;
(vi) sensitivity norms $\|\partial u/\partial \theta j\|$;
(vii) uncertainty intervals when data are noisy.

Table 9: Minimum Reproducibility Checklist for Computational Experiments

Item	Required Information
Model definition	Kernel, forcing, delay convention, boundary and initial data.
Discretization	Grid, basis or collocation nodes, quadrature and discrete regularizer.
Nonlinear solve	Algorithm, initialization, damping, stopping tests and maximum iterations.
Parameter selection	Rule used for ε, calibration bounds and prior values.
Validation	Independent cases, error metrics and uncertainty treatment.
Software	Language, package versions and scripts needed to regenerate figures and tables.
Data status	Clear distinction between synthetic, public experimental and proprietary data.

Limitations and Open Mathematical Problems
The present framework is intentionally reduced and several limitations remain. First, a scalar Urysohn equation cannot represent all spatial flame structures, particle-scale heterogeneity or multiphase transport. Second, the contraction condition is sufficient rather than necessary and may be conservative near bifurcation. Third, the current spectral analysis is based on linearization and does not fully characterize nonlinear transient growth. Fourth, experimental calibration is not supplied in the present synthetic study.

Important open problems include the following. One is the construction of global attractors for nonlocal combustion equations with state-dependent delay. Another is the characterization of Hopf bifurcation when the linearized Urysohn operator is nonnormal. A third is adaptive regularization with rigorous convergence under simultaneous discretization and data noise. A fourth is the derivation of error bounds for neural operators constrained by causal integral equations.

Finally, multidimensional AP/HTPB models require coupled thermal, chemical, mechanical and acoustic fields with uncertain interfaces.

A particularly interesting direction is the pseudospectral analysis of the discrete Jacobian. Even when all eigenvalues lie inside the unit disk, nonnormality may produce large transient amplification. Bounds involving the Kreiss constant or resolvent integrals could connect transient growth with ignition sensitivity and pressure oscillations.

Implementation Workflow and Pseudocode
The complete numerical workflow combines parameter continuation, a nonlinear solver and posterior diagnostics. The following sequence is recommended. First, nondimensionalize all inputs and assemble the causal quadrature weights. Second, construct the discrete positive regularizer L_h and verify that its smallest eigenvalue is nonnegative. Third, choose an initial regularization value from the spectral-margin rule. Fourth, solve the regularized nonlinear system and decrease ε by continuation until the discrepancy or bias criterion is reached. Finally, compute sensitivities, leading eigenvalues and uncertainty indicators using the converged state.

Step 1: Select the grid, quadrature rule, physical parameters and admissible interval $[\varepsilon_{\min}, \varepsilon_{\max}]$.

Step 2: Form the residual $F_{\varepsilon,h}(u) = u + \varepsilon L_h u - f_h - U_h(u)$ and its Jacobian.

Step 3: Initialize $u^0 = f_h$ or use the converged solution from a larger regularization value.

Step 4: Apply damped Newton; use Picard iteration as a fallback when the Jacobian step fails the descent test.

Step 5: Stop when both the residual and relative increment satisfy their tolerances.

Step 6: Estimate $r(B_{\varepsilon,h})$, $\kappa(F'_{\varepsilon,h})$ and the data discrepancy.

Step 7: Reduce ε only when the stability margin remains above the prescribed threshold.

Step 8: Solve the sensitivity equations and store all diagnostics needed to reproduce tables and figures.

A robust hybrid update can be written as

$$u^{k+1} = u^k + \lambda_k s_N^k + (1-\lambda_k) s_P^k, \tag{22.1}$$

where s_N^k is the Newton correction and

$$s_P^k = R_{\varepsilon,h}(f_h + U_h(u^k)) - u^k \tag{22.2}$$

is the Picard correction. When the Jacobian is well conditioned and the Newton model predicts sufficient decrease, λ_k is close to one. Near a singular or poorly initialized regime, reducing λ_k moves the method toward the globally safer fixed-point direction.

The final computational record should contain ε, h, the number of nonlinear and linear iterations,final residual, spectral radius estimate, condition number estimate, and a checksum or version identifier for the input data. This small amount of metadata is sufficient to detect most accidental inconsistencies between manuscript tables, source code and regenerated figures.

Detailed Proof of Compactness for the Causal Urysohn Operator
We provide the compactness argument used implicitly in the existence theory. Let $B_r = \{u \in C(I) : \|u\| \le r\}$. By the growth condition,

$$|(Uu)(t)| \le \int_0^t a(s)(1+r)\,\mathrm{d}s \le (1+r)\|a\|_{L^1(I)}, \tag{A.1}$$

so $U(B_r)$ is uniformly bounded. To prove equicontinuity, let $0 \le t_1 < t_2 \le T$. Then

$$|(Uu)(t_2) - (Uu)(t_1)| \le \int_0^{t_1} |K(t_2,s,u(s)) - K(t_1,s,u(s))|\,\mathrm{d}s \tag{A.2}$$

$$+ \int_{t_1}^{t_2} |K(t_2,s,u(s))|\,\mathrm{d}s. \tag{A.3}$$

The second integral tends to zero uniformly in $u \in B_r$ by absolute continuity of the Lebesgue integral. For the first, continuity of K in t on bounded state sets and dominated convergence imply uniform convergence to zero as $t_2 - t_1 \to 0$. Hence $U(B_r)$ is equicontinuous. The Arzelà–Ascoli theorem shows that its closure is compact in $C(I)$.

If the kernel is only measurable in t, compactness can still be obtained in $L^p(I)$under appropriate translation estimates. For spatially distributed kernels, the same reasoning is applied in the product variables (x, t), using compact embeddings or the Fréchet–Kolmogorov criterion.

Lemma A.1 (Compactness after regularization). *If $R_\varepsilon = (I+\varepsilon L)^{-1}$ is compact and U is continuous and bounded on bounded sets, then $T_\varepsilon = R_\varepsilon(f + U(\cdot))$ is compact on bounded subsets of X.*

Proof. For a bounded sequence u_n, the sequence $f + U(u_n)$ is bounded. Compactness of R_ε yields a convergent subsequence of $R_\varepsilon(f + U(u_n))$.

Newton, Damped Newton and Levenberg–Marquardt Algorithms
Define the nonlinear residual

$$F_\varepsilon(u) = u + \varepsilon Lu - f - U(u). \tag{B.1}$$

The Fréchet derivative is

$$F'_\varepsilon(u) = I + \varepsilon L - DU(u). \tag{B.2}$$

For the kernel (2.2), the state derivative is

$$(DU(u)v)(t) = \int_0^t \alpha e^{-\beta(t-s)} \frac{1-\gamma u(s)^2}{(1+\gamma u(s)^2)^2}(1+\eta p(s)^m) v(s)\,\mathrm{d}s. \tag{B.3}$$

Newton Iteration
Given u^k, solve

$$F'_\varepsilon(u^k)s^k = -F_\varepsilon(u^k), \qquad u^{k+1} = u^k + s^k. \tag{B.4}$$

Local quadratic convergence follows when F'_ε is Lipschitz continuous and $F'_\varepsilon(u_\varepsilon)$ is invertible. In practice, the linear system is dense because of the integral term, although causality produces a lower-triangular structure under time marching.

Damped Newton Iteration

A globalization parameter $\lambda_k \in (0,1]$ is selected so that

$$\|F_\varepsilon(u^k + \lambda_k s^k)\| \le (1 - c\lambda_k)\|F_\varepsilon(u^k)\|, \tag{B.5}$$

with $c \in (0, 1)$. Backtracking starts from $\lambda_k = 1$ and repeatedly multiplies it by a factor $\rho \in (0, 1)$.
This method retains fast local convergence while protecting against poor initial guesses.

Levenberg–Marquardt Calibration

For a data residual $r(\theta) = Cu_\varepsilon(\theta) - y,$ the parameter update solves

$$(J_k^T W J_k + \lambda_k I)d^k = -J_k^T W r(\theta^k), \tag{B.6}$$

where J_k is the sensitivity matrix. Large λ_k produces a gradient-like step; small λ_k approaches Gauss–Newton. A trust-ratio test compares actual and predicted decrease to update λ_k.

Table 10: Recommended Stopping Tests for Nonlinear and Inverse Iterations

Test	Condition	Interpretation
Residual	$\|F_\varepsilon(u^k)\| \le \tau_F$	The discrete equation is satisfied to tolerance.
Increment	$\|u^{k+1} - u^k\| \le \tau_u(1 + \|u^{k+1}\|)$	Further iterations change the state negligibly.
Data discrepancy	$\|Cu^k - y^\delta\| \le \tau\delta$	The fit is consistent with the noise level.
Gradient	$\|J_k^T W r_k\| \le \tau_g$	Approximate first-order stationarity in calibration.
Iteration cap	$k \ge k_{\max}$	Protection against stagnation or model failure.

Nondimensionalization of a Reduced Combustion Model

Consider a characteristic temperature difference ΔT, time scale t_c, pressure scale p_C and burning-rate scale r_c. Introduce

$$\vartheta = \frac{T - T_0}{\Delta T}, \qquad \xi = \frac{t}{t_c}, \qquad \pi = \frac{p}{p_c}, \qquad \rho_b = \frac{r_b}{r_c}. \tag{C.1}$$

A reduced thermal-memory equation can be written as

$$\frac{\mathrm{d}\vartheta}{\mathrm{d}\xi} + \mathrm{Bi}\,\vartheta = \mathrm{Da}\,\pi^n \exp\!\left(-\frac{\Theta}{1 + \delta_T\vartheta}\right) + \mathrm{Me}\int_0^\xi e^{-\mathrm{De}(\xi - s)}\Phi(\vartheta(s), \pi(s))\,\mathrm{d}s. \tag{C.2}$$

Here Bi is an effective thermal-loss number, Da is a reaction-to-transport ratio, $\Theta = E/(R_g T_0)$ is an activation parameter, Me is the memory intensity and $\mathrm{De} = \beta t_c$ is the dimensionless memory-decay rate.

The nondimensional groups clarify parameter interactions. Large Da and Θ promote sharp temperature sensitivity. Large Bi stabilizes the thermal state. Small De corresponds to persistent memory and can strengthen delayed feedback. The regularization parameter becomes

$$\varepsilon_* = \varepsilon \frac{\ell_L}{t_c}, \tag{C.3}$$

where ℓ_L depends on the scaling of L. Reporting dimensionless parameters improves comparison across propellant formulations and experimental facilities.

A Worked Scalar Example

Consider

$$u(t) + \varepsilon u(t) = f(t) + \alpha \int_0^t e^{-\beta(t-s)} \tanh(u(s))\,\mathrm{d}s, \qquad 0 \le t \le T. \tag{D.1}$$

Here $L = I$, and the resolvent is multiplication by $(1+\varepsilon)^{-1}$. Since $|\tanh'(z)| \le 1,$

$$\|Uu - Uv\| \le \alpha \frac{1 - e^{-\beta T}}{\beta}\|u - v\|. \tag{D.2}$$

Therefore the regularized fixed-point map is a contraction whenever

$$q_\varepsilon = \frac{\alpha}{1+\varepsilon}\frac{1-e^{-\beta T}}{\beta} < 1. \tag{D.3}$$

Take $T = 5$, $\alpha = 0.7$, $\beta = 0.8$ and $\varepsilon = 0.1$. Then

$$q_\varepsilon \approx \frac{0.7}{1.1}\frac{1-e^{-4}}{0.8} \approx 0.781 < 1. \tag{D.4}$$

The Picard error is bounded by $0.781^n\|e_0\|$. After 20 iterations, the theoretical factor is below 7.2×10^{-3}. The bound is conservative because the derivative of tanh is substantially smaller than one away from the origin.

For the unregularized equation, the contraction factor is approximately 0.859. Regularization improves the contraction margin from $1 - 0.859$ to $1 - 0.781$. If the unregularized solution belongs to $D(L) = X$, Theorem 4.3 gives

$$\|u_\varepsilon - u\| \le \frac{\varepsilon}{1-q_0}\|u\|, \qquad q_0 = \alpha\frac{1-e^{-\beta T}}{\beta}. \tag{D.5}$$

This explicitly displays the trade-off: increasing ε accelerates iteration but increases bias linearly. Differentiating (D.1) with respect to α gives

$$(1+\varepsilon)u_\alpha(t) - \alpha\int_0^t e^{-\beta(t-s)}\,\mathrm{sech}^2(u(s))u_\alpha(s)\,\mathrm{d}s = \int_0^t e^{-\beta(t-s)}\tanh(u(s))\,\mathrm{d}s. \tag{D.6}$$

Thus sensitivity is obtained by solving another linear Volterra equation with the same stable left-hand operator as the Newton correction.

Notation and Symbols

Table 11: Principal Notation used in the Manuscript

Symbol	Meaning
X	Banach space of continuous or integrable state functions.
U_θ	Nonlinear causal Urysohn integral operator with parameter vector θ.
L	Positive regularization operator, possibly differential, fractional or graph based.
R_ε	Resolvent $(I + \varepsilon L)^{-1}$.
u	Solution of the unregularized integral equation.
u_ε	Regularized solution.
$u_{\varepsilon,h}$	Regularized and discretized solution.
K	Nonlinear integral kernel.
α	Memory or feedback intensity.
β	Exponential memory-decay parameter.
γ	Nonlinear saturation coefficient.
τ	Discrete or effective delay.
A_ε	Derivative $D_u U_\theta(u_\varepsilon)$.
B_ε	Regularized linearized map $R_\varepsilon A_\varepsilon$.
$r(B_\varepsilon)$	Spectral radius of B_ε.
κ_ε	Condition number of the linearized regularized operator.
h	Discretization scale.
p	Approximation order or, when explicitly stated, pressure.
C	Observation operator mapping states to measurable quantities.
S	Sensitivity matrix.
$\mathcal{I}$	Fisher information matrix.
δ	Measurement-noise level.
δ_K	Kernel perturbation magnitude.

Recommended Validation Matrix

The theoretical and computational claims can be assessed through a structured validation matrix. Each row should be checked on at least three grid levels and, for experimental work, on independent datasets.

Table 12: Validation Matrix for Future Experimental and Computational Studies

Claim	Numerical test	Acceptance Indicator
Existence and boundedness	Run from several bounded initial guesses and parameter values.	All trajectories remain in the predicted invariant ball.
Uniqueness	Start Picard or damped Newton from separated initial states.	Convergence to the same discrete solution within tolerance.
Exponential stability	Plot iteration error or perturbed trajectory difference on a semilog scale.	Observed slope consistent with the predicted contraction bound.
O(ε) convergence	Compute against a highly resolved reference for a geometric sequence of ε.	Log-log slope near one in the asymptotic regime.
Kernel robustness	Perturb memory amplitudes and decay rates within controlled bounds.	State difference below the theoretical Lipschitz envelope.
Spectral stability	Compute leading eigenvalues and resolvent norms of the discrete Jacobian.	Spectrum inside the prescribed stability enclosure.
Discretization order	Repeat on grids h, h/2 and h/4.	Empirical order approaches the expected p.
Parameter sensitivity	Compare analytical sensitivities with centered finite differences.	Relative discrepancy decreases with the finite-difference step before roundoff.
Experimental prediction	Calibrate on one subset and validate on another.	RMSE, MAE and uncertainty coverage reported without data leakage.
Neural-operator surrogate	Compare against unseen forcing and parameter functions.	Stable residuals and controlled out-of-distribution degradation.

Discussion

The new results show that regularization does more than smooth numerical profiles. It changes the linearized spectrum, improves the resolvent bound and creates a quantitative stability margin. The estimate (4.6) separates modelling bias from discretization error. The robustness theorem controls uncertainty in the memory kernel, while parameter differentiability enables calibration and uncertainty propagation [1-51].

The numerical results indicate that long memory increases amplitude and slows convergence. Newton-type methods reduce iteration counts but require linear solves and a reliable initial guess. Levenberg–Marquardt is attractive when parameters are inferred from noisy combustion data. The spectral plots and heat map provide practical diagnostics for choosing ε. The present computational data and numerical results are synthetic and are intended solely to illustrate the theory. Experimental validation remains necessary before predictive use in a specific propellant formulation.

Conclusions

A regularized Urysohn operator provides a rigorous framework for nonlinear AP/HTPB combustion with hereditary effects. Existence, uniqueness, a priori bounds, exponential stability, kernel robustness, first-order convergence, parameter differentiability, spectral localization and pseudospectral control have been established. The numerical study covers short and long memory, strongly nonlinear kernels, several values of ε, solver comparisons and sensitivity to temperature and delay. Deep- ONet, FNO, physics-informed neural operators and transformer memory offer natural data-driven extensions.

Future work should combine laboratory AP/HTPB datasets with uncertainty quantification, multidimensional heat conduction, acoustic coupling, adaptive regularization and certified neural operators.

Acknowledgements

The authors gratefully acknowledge the invaluable scientific, academic, and material support provided by SPSU and PSNRU throughout the development of this research. The institutional environment, research infrastructure, access to computational resources, academic facilities, and continuous encouragement of scientific innovation created by SPSU were fundamental to the completion of this work. The authors particularly recognize PSNRU commitment to promoting advanced research in applied mathematics, mathematical modelling, engineering sciences, artificial intelligence, and interdisciplinary scientific collaboration.

The authors also express their sincere appreciation to the Instituto Superior de Ciênciase Tecnologia de Moçambique (ISCTEM) for its continuous scientific support and for fostering an academic environment that encourages high-level research in mathematics and its applications. The stimulating research atmosphere, scholarly discussions with colleagues, institutional encouragement, and access to academic resources significantly contributed to the theoretical development and refinement of the mathematical framework presented in this article.

The collaboration between SPSU, PSNRU and ISCTEM has provided an excellent interdisciplinary platform where mathematical analysis, computational methods, engineering applications, and emerging artificial intelligence techniques can be integrated to address complex real-world problems. Such institutional cooperation has been instrumental in advancing the present research on regularized Urysohn operators and their applications.

The authors further acknowledge the administrative staff, research colleagues, postgraduate students, and all members of both institutions whose support, constructive discussions, and encouragement contributed directly or indirectly to the successful completion of this work. Their commitment to academic excellence and scientific development has greatly enriched the quality of this research.

Finally, the authors express their sincere gratitude to the anonymous reviewers and the editors for their valuable comments, constructive suggestions, and careful evaluation of the manuscript, which substantially improved the clarity, mathematical rigor, and overall quality of the final publication.

Data Availability Statement
The numerical data and results used in this article are synthetic and can be regenerated from the equations and parameter tables presented in the manuscript. They should not be interpreted as experimental validation, and no confidential experimental dataset was used.

Funding
This research received no external funding.

Conflict of Interest
The authors declare that they have no conflict of interest.

References
1. Volterra V (1959) Theory of Functionals and of Integral and Integro-Differential Equations. Dover.
2. Krasnoselskii MA (1964) Topological Methods in the Theory of Nonlinear Integral *Equations. Pergamon*.
3. Tricomi FG (1985) Integral Equations. Dover.
4. Gripenberg G, Londen SO, Staffans O (1990) Volterra Integral and Functional Equations.Cambridge University Press.
5. Zeidler E (1986) Nonlinear Functional Analysis and Its Applications. Springer 27.
6. Pazy A (1983) Semigroups of Linear Operators and Applications to Partial Differential Equations. Springer.
7. Kato T (1995) Perturbation Theory for Linear Operators. Springer.
8. Trefethen LN, Embree M (2005) Spectra and Pseudospectra. Princeton University Press.
9. Engl HW, Hanke M, Neubauer A (1996) Regularization of Inverse Problems. Kluwer.
10. Tikhonov AN, Arsenin VY (1977) Solutions of Ill-Posed Problems. Winston.
11. Bakushinsky AB, Yu Kokurin M (2004) Iterative Methods for Approximate Solution of Inverse Problems. Springer https://link.springer.com/book/10.1007/978-1-4020-3122-9.
12. Atkinson K (1997) The Numerical Solution of Integral Equations of the Second Kind. Cambridge University Press doi.org/10.1017/CBO9780511626340.
13. Brunner H (2004) Collocation Methods for Volterra Integral and Related Functional Equations.Cambridge University Press doi.org/10.1017/CBO9780511543234.
14. Wazwaz AM (2011) Linear and Nonlinear Integral Equations. Springer https://link.springer.com/book/10.1007/978-3-642-21449-3.
15. Kuo KK, Summerfield M (1984) Fundamentals of Solid-Propellant Combustion. AIAA https://arc.aiaa.org/doi/book/10.2514/4.865671.
16. Williams FA (1985) Combustion Theory. CRC Press doi.org/10.1201/9780429494055.
17. Sutton GP, Biblarz O (2017) Rocket Propulsion Elements. Wiley 1-800.
18. Culick FEC (2006) Unsteady Motions in Combustion Chambers for Propulsion Systems. NATO RTO 10.14339/RTO-AG-AVT-039.
19. Lengellé G, Duterque J, J Trubert F (2000) Combustion of solid propellants, in Solid Propellant Chemistry, Combustion, and Motor Interior Ballistics, AIAA.
20. Beckstead MW (2006) Recent progress in modeling solid propellant combustion, Combustion,Explosion, and Shock Waves 42: 623-641.
21. Price EW (1984) Combustion of metallized propellants, in Kuo and Summerfield.
22. Raun RL, Beckstead MW (1993) A numerical model for combustion of AP composite propellants, Combustion and Flame 94: 1-24.
23. Ward MJ, Son SF, Brewster MQ (1998) Steady deflagration of HMX with simple *kinetics, Combustion and Flame* 114: 556-568.
24. Lu L, Jin P, Pang G, Zhang Z, Karniadakis GE (2021) Learning nonlinear operators via DeepONet, Nature Machine Intelligence 3: 218-229.
25. N Kovachki, Li Z, Liu B, Azizzadenesheli K, Bhattacharya K, et al. (2023) Neural operator: learning maps between function spaces with applications to PDEs, Journal of Machine Learning Research 24: 1-97.
26. Z. Li, Kovachki NB, Azizzadenesheli K, liu B, Bhattacharya K, et al. (2021) Fourier neural operator for parametric partial differential equations. ICLR.
27. Li Z, Zheng H, Kovachki N, Jin D, Chen H, et al. (2024) Physics-informed neural operator for learning partial differential equations. ACM/JMDS 28.
28. Goswami S, Bora A, Yu Y, Karniadakis GE (2022) Physics-informed deep neural operator networks arXiv:2207.05748.
29. Karniadakis GE, Kevrekidis IG, Lu L, Perdikaris P, Wang S, et al. (2021) Physics-informed machine learning, Nature Reviews Physics 3: 422-440.
30. Raissi M, Perdikaris P, Karniadakis GE (2019) Physics-informed neural networks, Journal of Computational Physics 378: 686-707.
31. Wang S, Teng Y, Perdikaris P (2021) Understanding and mitigating gradient pathologies in PINNs, SIAM Journal on Scientific Computing 43: A3055-A3081.
32. Z Hao, Su C, Liu S, Berner J, Ying C, et al. (2024) DPOT: auto-regressive denoising operator transformer for large-scale PDE pre-training. PMLR 235: 17616-17635.
33. Chen J, Wu K (2024) Position-induced transformer for operator learning, PMLR 235.
34. Xiao Z, Hao Z, Lin B, Deng Z, Su H (2024) Improved operator learning by orthogonal attention, PMLR 235: 54288-54299.
35. Liu-Schiaffini M, Berner J, Bonev B, Kurth T, Azizzadenesheli K, et al. (2024) Neural operators with localized integral and differential kernels, PMLR 235.
36. Cheng Z, Hao Z, Wang X, Huang J, Wu Y, et al. (2024) Reference neural operators, PMLR 235.
37. Pal S, Adepu H, Wang C, Golland P, Singh V (2024) Implicit representations via operator learning, PMLR 235.
38. Lin B, Mao Z, Wang Z, Karniadakis GE (2023) Operator-learning-enhanced PINNs for sharp solutions arXiv:2310.19590.
39. Zhu M, Feng S, Lin Y, Lu L (2023) Fourier-DeepONet for full waveform inversion arXiv:2305.17289.
40. Li W, Bazant MZ, Zhu J (2023) Phase-Field DeepONet arXiv:2302.13368.
41. Gracyk A, Chen X (2024) GeONet: a neural operator for Wasserstein geodesics, PMLR 244: 1453-1478.
42. Dong H, Wang H, Liu H, Luo J, Wang J (2024) Accelerating PDE data generation via differential operator action in solution space, PMLR 235: 11395-11411.
43. Chakraborty S, Nelakanti G (2025) Jacobi spectral methods for nonlinear Volterra–Urysohn integral equations, Journal of Mathematical Analysis and Applications 543.

44. Kumar S (2024) Kantorovich methods for Urysohn integral equations, in Computational Methods for Integral Equations. Springer.
45. Alves MJ (2025) Continuity properties of Urysohn operators in functional spaces. Functional Differential Equations 32.
46. Alves MJ (2026) Regularization of second-order functional differential equations in weighted spaces, Journal of Physical Mathematics and its Applications 4.
47. Molchanova Alves EV, Alves MJ (2026) Non-stationary combustion in solid propellants incorporating time delays and memory effects, accepted manuscript 29.
48. Renardy M, Rogers RC (2004) An Introduction to Partial Differential Equations. Springer.
49. Kreyszig E (1978) Introductory Functional Analysis with Applications. Wiley.
50. W. Rudin (1991) Functional Analysis, McGraw-Hill.
51. Deimling K (1985) Nonlinear Functional Analysis. Springer.